Quantum Confinement Effects Enable Photocatalyzed Nitrate Reduction at Neutral pH Using CdS Nanocrystals

Brian A. Korgel[†] and Harold G. Monbouquette*

Chemical Engineering Department, 5531 Boelter Hall, Box 951592, University of California, Los Angeles, Los Angeles, California 90095-1592

Received: March 20, 1997[⊗]

Size-quantized CdS nanocrystals serve as photocatalysts for nitrate reduction at neutral pH under conditions that mimic illumination by sunlight with overall product quantum yields of up to 4% for ~20 Å, amine-terminated particles. Due to the effects of quantum confinement on electron and hole redox potentials, photocatalyzed nitrate reduction rates depend strongly on the apparent particle size, and the fastest reduction rates are observed with the smallest nanocrystals which have the highest exciton energy. Using a Tafel plot and the empirical pseudopotential model to estimate electron redox potentials, the apparent electron transfer coefficient and the apparent standard rate constant are estimated at 0.23 and 4.0×10^{-12} cm/s, respectively, for amine-terminated particles. The apparent values for these constants indicate sluggish kinetics and the probable influence of adsorption and double-layer effects on the observed reaction rate. The effect of nitrate adsorption on photoreduction rates is described well by a Langmuir−Hinschelwood expression. Nitrate reduction rates are reduced 2-fold or more on negatively charged, carboxy-terminated nanocrystals that electrostatically repel nitrate. Chloride competes with nitrate for access to particle surfaces, and reduced photoreduction rates are observed for both amine- and carboxy-terminated particles with increased NaCl concentration. The rate of photocatalyzed nitrate reduction on the amine-capped particles goes through a minimum at about pH 6.5, whereas the efficiency of nitrate reduction for the carboxy-terminated system decreases monotonically with increasing pH. In the absence of an electron donor other than water, rapid photocorrosion is observed; therefore, formate is used as the sacrificial electron donor in this study.

Introduction

Numerous studies have shown that semiconductor colloids can serve as photocatalysts for a variety of molecular synthesis and degradation reactions in solution.[1−4] Great interest has developed particularly in semiconductor materials that absorb light in the visible part of the energy spectrum since they may be driven efficiently by solar energy.[1−5] Use of submicron-size colloids that nearly eliminate light scattering losses and provide very high surface area to volume ratios has improved the efficiencies of most photocatalytic processes.[1−5] However, further improvement in quantum yields and increased electron transfer efficiency remains a major goal.[3,4]

A possible route to achieving higher quantum yields in photocatalytic applications may be through the use of size-quantized semiconductor nanocrystals for which the band gap is size-dependent. It is well-known that when the semiconductor nanocrystal diameter is comparable to or less than the bulk exciton diameter (approximately 60 Å for CdS), size-dependent optoelectronic properties and ionization potentials result.[6,7] Semiconductor nanoparticles exhibit lower ionization potentials as particle diameter is decreased beyond the threshold for quantum confinement.[8,9] Therefore, through particle size control, photocatalytic electron and hole redox potentials of size-quantized semiconductor nanocrystals can be tuned to achieve increased redox power for use in waste water decontamination, or in solar cells, or for selective synthesis processes.[1−5] Additionally, the wave function of an excited electron spreads over the entire size-quantized nanocrystal making it possible for every excited charge carrier to reach the surface before recombination.[5] Quantum yields of one are theoretically possible provided that surface and core traps do not significantly contribute to electron−hole recombination and that the charge carrier can be scavanged from the nanocrystal surface faster than the recombination rate.[10] Increased photooxidation and photoreduction capability using quantum-sized nanocrystals has been observed for a number of different semiconductor chemistries,[9−28] including quantum yields up to 30% for H_2O_2 decomposition on size-quantized ZnO.[14]

Although a standard deviation about the mean size-quantized nanoparticle diameter of as little as ±1% is manifested as inhomogeneous broadening in optoelectronic properties,[29] most photocatalytic applications would not require such narrow size distributions. However, in order to maintain a reasonably monodisperse population and to control the average particle diameter, colloidal stabilizing agents are needed; consequently, nanocrystal surfaces usually are coated with capping ligands.[7] These ligands govern the surface character (both the chemistry and physical structure) which impact greatly the properties vital to photocatalytic applications, such as fluorescence lifetimes and quantum yields,[30−32] surface charge and ionicity,[33−35] particle solubility,[36,37] and flat-band redox potentials.[38,39] The capping ligands can affect reactant concentrations at the particle surface and effective potentials through adsorption and double-layer effects. In fact, it has been proposed that electron transfer from the semiconductor to the reactant can compete with electron−hole recombination only if the reactants are adsorbed on the particle surface,[40] and numerous studies indicate that reactant and product binding on the semiconductor surface significantly affects the electron transfer efficiency.[2−5,19,33,35,39,41−49] Since a significant amount of control over the surface character is possible, it is desirable to know quantitatively how the surface

[†] Current address: Department of Chemistry, University College Dublin, Belfield, Dublin 4, Ireland.

[⊗] Abstract published in *Advance ACS Abstracts,* June 1, 1997.

S1089-5647(97)01016-X CCC: $14.00

character will affect the quantum yield of a particular photocatalytic reaction.

Photocatalytic reduction of nitrate at neutral pH presents an important challenge. Nitrate contamination of the watershed in areas under intense agricultural use is a persistent problem. High nitrate levels promote the growth of algae, which upon its decay robs watersheds of the oxygen necessary for animal life. Unfortunately, nitrate has been found to be very stable chemically and difficult to reduce using unmodified electrodes even at very high overpotentials.[50,51] Electrocatalytic nitrate reduction has been achieved using electrodes modified with homogeneous catalysts, such as Co(III) or Ni(II) cyclams,[52] Ru(II) bipyridine,[53] Fe(III) porphyrin,[54] and underpotential-deposited cadmium on gold.[55,56] Electrodes modified with nitrate reductase coupled to a number of electron-transferring dyes have also proven relatively effective.[57,58] Photosensitized nitrate reduction has been reported using metal porphyrins (quantum yield, Φ, equal to 5.3×10^{-4}),[59] organic sensitizers (*N*-methylphenothiazine and *N*,*N*,*N*′,*N*′-tetramethylbenzidine),[60] TiO_2 ($\Phi = 0.005$,[61] $\Phi = 0.02$[62]), $Pt-TiO_2$ suspensions ($\Phi = 0.02$),[63] ZnS colloids ($\Phi = 0.013$ and Pt-loaded $\Phi = 0.003$),[64] a variety of metal oxides ($\Phi = 0.006$),[65] and nitrate reductase coupled to an organic sensitizer ($Ru(bpy)_3^{2+}$) and methyl viologen ($\Phi = 0.08$).[66] The highest quantum yield obtained in these studies used nitrate reductase as the catalyst.[66] The highest quantum yield achieved for the nonenzymatic photocatalytic systems was 2% for the TiO_2 and $Pt-TiO_2$ suspensions under acidic conditions.[62,63] Since nitrate reduction becomes significantly more difficult with increasing pH, many of these studies did not report nitrate reduction at neutral pH or higher.

Studies on the mechanism of nitrate reduction in aqueous media at pH close to 7.0 have shown that the initial electron transfer step from an electrode to nitrate forms the short-lived intermediate, NO_3^{2-},[50,51]

$$NO_3^- + e^- \rightarrow NO_3^{2-} \quad (1)$$

This initial electron transfer step reportedly has a standard redox potential of at least -1.1 V vs NHE at pH 7.0,[50] whereas the standard redox potential for the overall NO_3^-/NO_2^- couple is 0.43 V. Since the standard electron redox potential at pH 7.0 for bulk CdS (-0.8 V vs NHE)[3] is less negative than the standard redox potential for the initial electron transfer step to nitrate, photoreduction using bulk CdS is not favorable and has not been reported in the literature. A substantial kinetic barrier to reduction exists due to the large reorganization energy likely required to go from planar NO_3^- to the bent configuration of NO_3^{2-}.[60] Quantum confinement effects may offer a useful means to shift the electron redox potential to sufficiently negative values to promote facile nitrate reduction.

In this study, nitrate photoreduction using size-quantized CdS nanocrystals is described. The effects of apparent particle size and surface character on the reduction current are examined using nanocrystals of varied size and surface charge. By examining the rate dependence on nitrate, formate (sacrificial electron donor), NaCl concentration, and pH, the effects of the nanocrystal surface are further elucidated.

Experimental Section

Nanocrystal Preparation. Quantum-sized CdS nanocrystals were synthesized at room temperature using arrested growth methods in aqueous solution with mercaptoacetic acid and/or 2-mercaptoethylamine (Sigma) serving as colloidal stabilizers.[37,67] Nanocrystals were prepared in a stirred solution of 0.027 g of $CdCl_2$ (1 mM) in 150 mL of pure water. Negatively charged nanocrystals were synthesized by lowering the solution pH to 2.8 with mercaptoacetic acid, raising the pH to 8.5 with concentrated NaOH, and finally adding 16.5 mL of 10 mM $Na_2S{\cdot}9H_2O$ (0.040 g). The solution turned yellow immediately after sulfide addition. The particle size depended on the pH value prior to sulfide addition, with larger particles forming at higher final pH values. By using 2-mercaptoethylamine as the capping agent instead of mercaptoacetic acid, particles with positively charged surfaces could be synthesized. After adding 0.378 g of 2-mercaptoethylamine to the initial 1 mM $CdCl_2$ solution, the pH was lowered to 7.8 by adding concentrated HCl. The solution turned a pale yellow color immediately after adding 16.5 mL of 10 mM $Na_2S{\cdot}9H_2O$ (0.040 g). Smaller nanocrystals were obtained at lower pH prior to sulfide addition. Mixed charge particles were synthesized by adding different molar ratios of mercaptoacetic acid and 2-mercaptoethylamine to the 1 mM $CdCl_2$ solution. After adding the capping agent to the solution, the pH was measured and adjusted to approximately 7.0 using either HCl or NaOH depending on the capping agent ratio used.

Experimental Setup. Photocatalysis experiments were performed at room temperature using 1.0 mL of the freshly prepared CdS colloidal suspension added to 4.0 mL of 50 mM phosphate buffer at pH 7.0, which corresponds to a CdS concentration of approximately 0.014 wt %. $NaNO_3$ was added to the buffered solutions at desired concentrations, and the solution was sparged with Ar to remove oxygen. The pH was varied for some experiments using 50 mM phosphate buffer at the desired pH value. Sodium formate was added to the reaction mixture to serve as a sacrificial electron donor. In some cases NaCl was added to study the effects of ionic strength and Cl^- concentration on the reaction. After initial sparging with Ar, the reaction mixture was illuminated with a 150 W Hg/Xe lamp (Osram XBO) used in conjunction with an 800 nm infrared cutoff filter (Oriel) to eliminate heating effects. The light intensity in all the experiments was 40 mW/cm^2 as determined using a thermopile (Eppley Laboratory, Inc., Newport, RI). This measured light intensity compared to within 10% of that measured using a standard actinometric method (photolysis of Reinecke salt).[68] Nitrite concentrations after photocatalysis were measured by diazotization with sulfanilamide and coupling with *N*-(1-naphthyl)ethylenediamine.[69]

Quantum Yield Calculations. In this study, initial overall quantum yields, Φ, are reported as the total moles of nitrite formed divided by one-half the total moles of photons absorbed, since nitrate reduction to nitrite is a two-electron process. Nitrite concentrations in the reaction mixture were measured after 15 min of continuous light exposure. Photon absorption was calculated from the light intensity, the emission spectra of the lamp, and the absorption spectra of the reaction mixture with proper accounting of nitrate absorption ($\lambda_{max} \sim 300$ nm). The nanocrystal suspensions used in these experiments were transparent, and light-scattering losses were negligible. In order to simulate solar conditions, UV cutoff filters or band-pass filters were not employed, and the sample absorbed photons with energies spanning its entire absorption spectra down to 280 nm, at which point the borosilicate tubes used for the reaction mixture cut off light transmission. Photocatalytic nitrite reduction was not considered in the quantum yield calculations. Although nitrite reduction was found to occur at a rate similar to that for nitrate, nitrite formation after 15 min of light exposure was on the order of 0.02 mM, and the rate of nitrite consumption at these very low concentrations is negligible compared to the rate of nitrite formation.

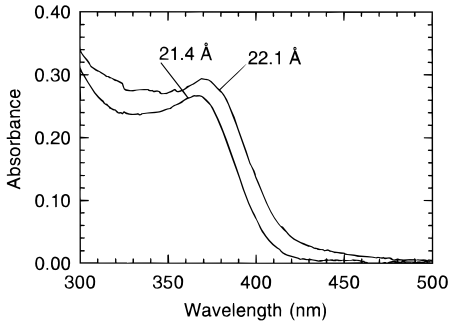

Figure 1. Typical room temperature optical absorption spectra of two approximately 0.014 wt % CdS nanocrystal dispersions prepared using amine capping. The relatively narrow peak width indicates good particle quality and a relatively tight size distribution for all preparations. The difference in average particle size between the two samples is evident in the shift of both the absorbance edge and the exciton peak energies.

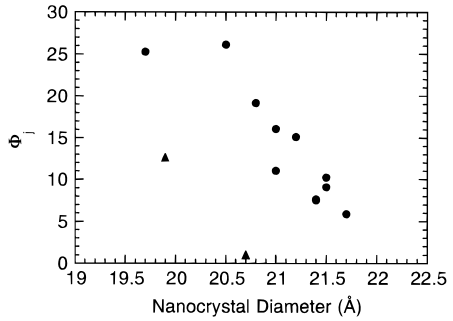

Figure 2. Current density quantum yield, Φ_j, versus the particle diameter for (●) amine-capped and (▲) carboxy-capped nanocrystals.

To account for differences in total surface area between suspensions of nanocrystals of different size, the current density quantum yield, Φ_j (Φ_j = amps per nanocrystal surface area per mole photons absorbed), was calculated by multiplying Φ by the Faraday constant and dividing by the total surface area of the sample per milliliter of reaction solution. The surface area of the sample was estimated based upon the initial Cd concentration and the average apparent particle diameter determined from UV−visible absorption spectra (see below), assuming complete reaction during particle growth.

UV−Visible Absorption Spectra and Size Estimation. Nanocrystal spectra were gathered for the reaction mixture prior to light exposure using a Beckman DU-65 spectrophotometer (scan rate = 500 nm/min). From these spectra, the total photons absorbed during light exposure was calculated.

Average apparent nanocrystal diameters were estimated from the exciton energies determined from the UV−visible absorption spectra (Figure 1) using the empirical pseudopotential model[70] for hexagonal CdS nanocrystals,[71,72] since it has been shown that CdS particles formed by the method used have hexagonal structure.[67] Size distribution effects on reaction rates were not considered throughout the study since standard deviations about the mean particle diameter for samples prepared as above have been reported to be less than 10%.[37] The sharpness of the exciton peaks in UV−visible absorption spectra such as that of Figure 1 also indicates that particles are monodisperse and crystalline.

Results and Discussion

Nanocrystal Size Dependence of Nitrate Photoreduction. As shown in Figure 2, the current density quantum yield, Φ_j, for nitrate photoreduction strongly depends on the apparent particle size. For these ~20 Å amine-capped nanocrystals, Φ_j increases by approximately 5-fold for a decrease in particle diameter of only 2 Å. The same trend is observed for the carboxy-terminated particles, although the quantum yields reproducibly ranged from unmeasurable to almost one-half of the amine-terminated nanocrystals. Nitrate photoreduction occurs with the use of mixed carboxy- and amine-capped nanocrystals as well; however, these particles precipitated during light exposure, and a meaningful quantum yield could not be obtained. Either the capping efficiency with the mixed ligands is insufficient or reduced electrostatic repulsion between particles enables aggregation and precipitation.

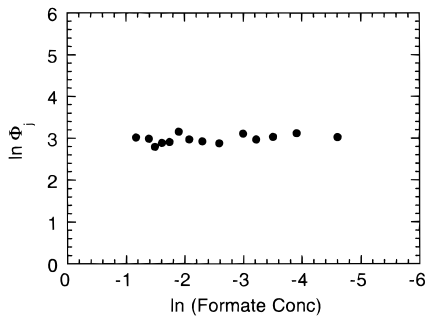

Figure 3. Current density quantum yield, Φ_j, dependence on formate concentration for amine-capped 20.7 Å CdS nanocrystals in 250 mM nitrate at pH 7.0.

Nitrate reduction rates using the amine-capped nanocrystals range from 6.7×10^{-7} μmol/(s cm^2) (0.13 μA/cm^2) for the smaller particles to 1.6×10^{-7} μmol/(s cm^2) (0.03 μA/cm^2) for the larger particles. For CdS nanocrystals in this size range (the particle diameter is substantially smaller than the bulk CdS exciton diameter of ~60 Å), slight decreases in apparent particle diameter significantly decrease the ionization potential due to quantum confinement effects.[8] Since the ionization potential corresponds to the electron redox potential, decreased particle diameter increases the reducing power of the electrons, resulting in an increased energetic driving force for electron transfer.[8,73,74] Therefore, the observed increase in reduction capability exhibited by the smaller nanocrystals in Figure 2 results directly from quantum confinement effects.

In general, the photocatalytic reaction rate can be influenced by the reaction of both the photogenerated electron and hole. In the absence of nanocrystal photocorrosion, both an electron and a hole must react at the surface of a single nanocrystal in order to maintain charge neutrality. In this system the hole acceptor (or sacrificial electron donor) is formate. By plotting the current density quantum yield for nitrate photoreduction against the formate concentration, the effect of hole transfer relative to electron transfer on the overall nitrate reduction rate may be determined. Figure 3 shows the natural log of Φ_j plotted against the natural log of formate concentration for 20.7 Å amine-capped CdS nanocrystals in 250 mM nitrate at pH 7.0. The rate is virtually independent of the formate concentration, showing that, under these experimental conditions and this nitrate concentration, hole transfer is facile compared to electron transfer, and nitrate reduction rates apparently are limited solely by the rate of electron transfer.

In fact, Figure 3 suggests that the presence of formate is not required to achieve nitrate photoreduction. However, the nanocrystal UV−visible absorption spectra in Figure 4 show that, without formate in solution, irradiation significantly decreases the nanocrystal dispersion absorbance due, presumably, to photocorrosion. No change in absorbance before and after irradiation was observed with formate present. Therefore, in order to eliminate catalyst loss, a suitable sacrificial electron donor is needed in solution, despite the fact that electron transfer

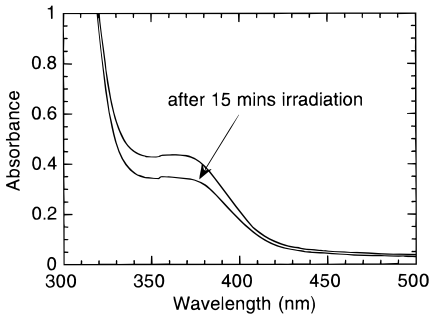

Figure 4. Room temperature UV−visible absorption spectra for approximately 0.014 wt % amine-capped CdS nanocrystals before and after nitrate reduction without formate (250 mM sodium formate) in a buffered (pH 7.0) 100 mM nitrate solution sparged with Ar.

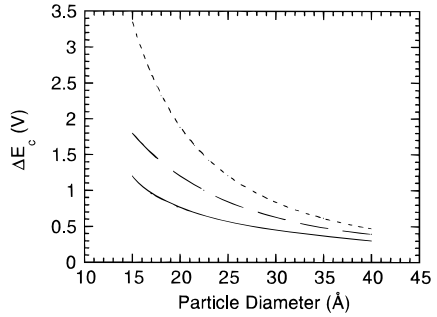

Figure 5. Shift in conduction band energy plotted versus particle diameter as predicted by the (—) tight-binding model,[74] (− −) the empirical pseudopotential model for wurtzite CdS,[73] and the (- - -) effective mass approximation.[8] The shift in conduction band energy is believed to correspond to the size-dependent shift in the electron redox potential.

is the rate-limiting step for nitrate photoreduction under the experimental conditions investigated.

In the absence of reactant adsorption and double-layer effects, and at sufficiently high overpotentials to render the anodic current (e.g., electron transfer from the initially reduced nitrate back to the particle surface) insignificant compared to the cathodic current, the current−potential dependence for an electrochemical reduction on a CdS nanoparticle can be expressed as[19,75,76]

$$j = nFk'^{\circ}C_{NO_3}(0,t)e^{-\alpha' nf(E(CdS,d)-E'^{\circ})} \quad (2)$$

In (2), j is the current density, n is the number of electrons transferred, F is the Faraday constant, f is F divided by the gas constant times the temperature, F/RT, k'° is the apparent standard rate constant, $C_{NO_3}(0,t)$ is the nitrate concentration at the nanocrystal surface, α' is the apparent electron transfer coefficient, and $E(CdS,d) - E'^{\circ}$ is the effective overpotential. Here, E'° is the standard redox potential for the rate-limiting electron transfer step for nitrate reduction to nitrite, and $E(CdS,d)$ is the electron redox potential in the nanocrystal, which depends on the particle diameter, d. Of course, in the system under investigation, with charged reactants and semiconductor surfaces with charged chemisorbed ligands, the influence of a double layer and nitrate adsorption cannot be neglected *a priori*; therefore, k'° and α' must be regarded as apparent constants in this formulation. In the absence of adsorption, charge double layer, and mass transfer effects, $C_{NO_3}(0,t)$ is equal to the bulk solution nitrate concentration, $C^*_{NO_3}$, and (2) becomes the Butler−Volmer equation for the cathodic reaction,

$$j = nFk'^{\circ}C^*_{NO_3}e^{-\alpha' nf(E(CdS,d)-E'^{\circ})} \quad (3)$$

The importance of mass transfer compared to the kinetics can be determined by examining the dimensionless Damkohler number:

$$Da = k_r/k_m \quad (4)$$

where k_r (cm/s) is the rate constant and k_m (cm/s) is the mass transfer coefficient. From (2) k_r is defined as

$$k_r = k'^{\circ}e^{-\alpha' nf(E(CdS,d)-E'^{\circ})} \quad (5)$$

and k_m for a sphere of diameter, d, in the absence of convection is

$$k_m = 2.0(D_{NO_3}/d) \quad (6)$$

where D_{NO_3} is the diffusion coefficient for nitrate. Using $k'^{\circ} = 4.0 \times 10^{-12}$ cm/s and $\alpha' = 0.23$ (as determined following the discussion below), with $n = 1$ and $E(CdS,\sim 20\ Å) - E'^{\circ} = -0.9$ vs NHE for 20 Å particles (see below), gives $k_r = 1.3 \times 10^{-8}$ cm/s. For a 20 Å diameter nanocrystal, $D_{NO_3} = 2 \times 10^{-5}$ cm^2/s, and $k_m = 100$ cm/s, $Da \cong 1 \times 10^{-10}$. A Da much less than one indicates that mass transfer to the particle surface is much faster than the reaction rate and can be neglected in the analysis.

According to Brus,[8] the electron redox potential of the nanocrystal is related to the size-dependent shift in the conduction band energy, $\Delta E_c(d)$, and (3) becomes

$$j = nFk'^{\circ}C^*_{NO_3}e^{-\alpha' nf(E(CdS,bulk)-\Delta E_c(d)-E'^{\circ})} \quad (7)$$

As described above, kinetic studies on the mechanism of nitrate reduction in aqueous media at pH close to 7.0 have shown that the initial electron transfer step from an electrode to nitrate forms the short-lived intermediate, NO_3^{2-}. Assuming that this initial electron transfer is rate-limiting, n in the exponential term in (7) is 1, and E'° is taken for the NO_3^-/NO_3^{2-} redox couple, which has a value of at least −1.1 V vs NHE at pH 7.0.[50] Since the overall reaction requires the transfer of two electrons, n in the preexponential term of (7) is 2, and the logarithm of (7) becomes[76]

$$\ln(j) = \ln(2Fk'^{\circ}C^*_{NO_3}) - \alpha' f[E(CdS,bulk) - \Delta E_c(d) - E'^{\circ}(NO_3^-/NO_3^{2-})] \quad (8)$$

From (8), α' and k'° can be determined from the slope and the y intercept of a Tafel plot of $\ln(j)$ versus $E(CdS,bulk) - \Delta E_c(d) - E'^{\circ}(NO_3^-/NO_3^{2-})$ given an appropriate estimate for $\Delta E_c(d)$.

A number of models for calculating $\Delta E_c(d)$ have been proposed with widely varying results (see Figure 5).[8,73,74] Since the empirical pseudopotential model[70] has been found to predict the exciton energy size dependence for CdS nanocrystals with the greatest accuracy,[71,77] $\Delta E_c(d)$ is calculated using this model, assuming hexagonal core structure.[71−73] As shown in Figure 5, estimates for $\Delta E_c(d_p)$ range from about 0.4 V for 40 Å particles to 1.8 V for 15 Å CdS nanocrystals, whereas $E(CdS,bulk)$ was taken from the literature to be −0.8 V vs NHE at pH 7.0.[3]

From (8), and the slope and y intercept of the best fit line in Figure 6, α' and k'° were estimated at 0.23 ($0.13 < \alpha' < 0.33$ with 95% confidence) and 4.0×10^{-12} cm/s ($1.7 \times 10^{-12} < k'^{\circ} < 9.0 \times 10^{-11}$ with 95% confidence), respectively. Again, these parameters represent apparent values since adsorption and charge double-layer effects were ignored for their determination.

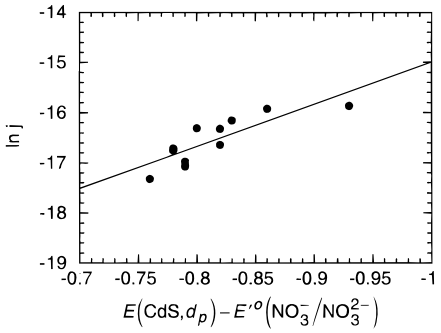

Figure 6. Tafel plot of the natural log of the measured current density versus the reaction overpotential for amine-capped CdS nanocrystals. The slope and intercept of the best-fit line give $\alpha' = 0.23$ and $k'^{\circ} = 4.0 \times 10^{-12}$ cm/s, respectively.

These parameters also depend, of course, on the model used to determine the shift in electron redox potential with size.

A value of α less than 0.5 indicates asymmetry in the energy barrier for this redox reaction such that the barrier to the cathodic reaction changes less with imposed potential than that for the anodic.[76] Normally, an α of 0.5 is expected. However, in this case a straightforward interpretation of the value obtained is not possible since the quantity measured is the apparent transfer coefficient. As discussed below, the presence of a double layer could affect the apparent value of α.

An apparent standard rate constant on the order of 10^{-12} cm/s indicates sluggish kinetics. Values of k° for metal electrodes typically range from 10^{2} to 10^{-4} cm/s.[42] However, this value for the rate constant, as with that for the transfer coefficient above, is an apparent one that has not been corrected for double-layer effects or adsorption. Nevertheless, a k'° equal to 10^{-12} cm/s does not necessarily indicate unusually slow electron transfer. Lewis[42] explains low rate constants in terms of the relatively low electron densities found on semiconductor surfaces rather than sluggish electron transfer alone. In comparison, a standardized rate constant for methyl viologen reduction on ~100 Å TiO_2 was found to be 2×10^{-17} cm/s,[75] and k° on the order of 10^{-12} cm/s has been measured for other semiconductor electrode systems.[78]

A characteristic time for electron transfer, τ, can be estimated by considering the electron flux as a function of a bimolecular rate constant, k_{et}, the concentration of acceptor in solution, $[NO_3^-]$, and the electron concentration on the semiconductor surface, n_s,[42]

$$\text{flux} = k_{et}[NO_3^-]n_s = k_n n_s \tag{9}$$

The standard rate constant relates to k_{et} through the electron density at the semiconductor surface under equilibrium conditions, n_{so}:[42]

$$k^{\circ} = k_{et} n_{so} \tag{10}$$

where n_{so} is related to the effective conduction band electron density, N_c, by the expression[42]

$$n_{so} = N_c e^{(E(\mathrm{CdS},d)-E'^{\circ})/kT} \tag{11}$$

Finally, τ can be related to the particle diameter and the rate constant, k_n:[42]

$$\tau = d/2k_n \tag{12}$$

The major uncertainties in calculating τ lie in the estimation of n_{so}, since these semiconductors are in the quantum-size regime, and in $[NO_3^-]$, since reactant adsorption may give rise to an effective nitrate concentration significantly different from the bulk solution concentration. Nevertheless, as an approximation, τ can be calculated using $d = 20$ Å, $[NO_3^-] = 6.02 \times 10^{19}$ molecules/cm^3 (100 mM), $k'^{\circ} = 4.0 \times 10^{-12}$ cm/s, and $n_{so} = 1.5 \times 10^{5}$ cm^{-3} (by taking the conduction band electron density, N_c, as 1 electron per particle and $E(\mathrm{CdS},d) - E'^{\circ} = -1.0$ V),[79] which gives $\tau \approx 60$ ps. This result is surprising considering the relatively low value for k'° as compared, once again, to those typically measured for metal electrodes. However, electron transfer times to methyl viologen on the order of 20 and 100 ps have been measured for 40−50 Å CdS[41] and 100 Å TiO_2,[75,80] respectively. In fact, electron transfer rates on the picosecond time scale may be required in order to compete with electron−hole recombination rates which have been estimated to be ~40 ps for 20 Å diameter CdS nanocrystals.[40,81]

Though electron transfer may occur on a rapid time scale, the standard rate constant nonetheless is very low, and extremely large overpotentials of up to 1 V give modest quantum yields of 4% for the smallest amine-terminated CdS nanoparticles. This quantum yield, however, is not corrected for probable water reduction activity. The redox potential for photoexcited electrons in the ~20 Å particles is ~−1.7 V vs NHE, which is of sufficient magnitude for water reduction.

Calculation of a turnover number, k_{turn}, determined from the rate of reduction, provides another measure of the efficiency of nitrate reduction. The turnover number can be calculated by assuming that each nanoparticle functions as a reaction center in a manner similar to reaction centers in enzymes. Following this assumption, k_{turn} is the maximum reduction rate per particle and $k_{turn} = 1 \times 10^{-2}$ s^{-1} using the 19.7 Å amine-capped nanocrystals. (For 19.7 Å amine-capped nanocrystals, $\Phi_{j,\max} = 47.4$; the number of absorbed photons is 2.1×10^{-14} mol photons/(s mL); the total particle surface area is 120.1 cm^2/mL; and the particle concentration is 1.2×10^{-8} mol particles/mL.) Since these are the smallest nanocrystals used in this study, and considering that k_{turn} would decrease in value if the number of active sites on each particle is greater than 1, $k_{turn} = 1 \times 10^{-2}$ s^{-1} represents the upper limit of the turnover number for nitrate reduction using CdS nanocrystals as photocatalysts in this work. In comparison, the value for k_{turn} obtained above is approximately an order of magnitude lower than the typical range for enzymes of from 1 to 10^4 s^{-1} [82] and is far lower than the 100−300 s^{-1} observed for each Mo catalytic center of *E. coli* nitrate reductase.[83]

The validity of the rate data reported above is confirmed by control studies run without nanocrystals, nitrate, or light exposure, which showed that each component was necessary to achieve nitrate reduction. In the absence of formate, nanocrystal absorbance decreases upon light illumination, as shown in Figure 4, due to photodegradation of the nanocrystals. However, in the presence of formate, the UV−visible absorption spectra (both the shape and absorbance) did not change after 15 min of irradiation, eliminating the possibility of photocorrosion during light exposure and confirming that the particles were serving as true catalysts. Therefore, photocorrosion should not cloud the determination of the rate parameters.

Effect of the Surface Charge on the Electron Transfer Kinetics. Due to the presence of charged amine or carboxy-terminated ligands on the nanocrystal surfaces, electrostatic interaction with nitrate is expected to be of importance in this photocatalytic system. As shown in Figure 2, the current density quantum yield, Φ_j, indeed does depend strongly on the surface character, with negative capping decreasing Φ_j by a factor of 2 or more. This result concurs with several studies that have shown that the interactions between charge-modified CdS

nanocrystal surfaces and charged dyes play a major role in determining photocatalytic efficiencies.[19,33,34] In one recent report, the surface charge of CdS nanocrystals also influenced the reaction route in the photoreduction of CO_2.[35] Surface charge may contribute to double-layer effects and reactant adsorption which can affect both the reactant concentration near the particle surface and the effective electron redox potential of the semiconductor. In the following sections, the effects of adsorption and a double-layer potential on the reaction rate are considered.

(i) Double-Layer Effects. The presence of a double layer influences electron transfer rates by changing the effective overpotential and by altering the concentration of reactive ions at the surface. Specific chemisorption of the amine-terminated ligands makes the double-layer potential at the outer Helmholtz plane, ϕ_2, more positive and attractive to nitrate ions since the difference in nitrate concentration between the bulk and the outer Helmholtz plane, x_2, is given by[76]

$$C_{NO_3}(x_2,t) = C^*_{NO_3} e^{F\phi_2/RT} \tag{13}$$

whereas the carboxy-terminated ligands shift the double layer to more negative potential. The effective potential at the semiconductor surface, E_{eff}, also must include ϕ_2,[76]

$$E_{eff} = E(\text{CdS,bulk}) - \Delta E_c(d) - \phi_2 \tag{14}$$

From (14) it is evident that the positive charge due to the amine capping group will shift E_{eff} to more reducing potentials. Correcting (8) for double-layer effects using (13) and (14) gives

$$\ln(j) = f\phi_2 + \ln(2Fk_t^\circ C^*_{NO_3}) - \alpha f(E(\text{CdS,bulk}) - \Delta E_c(d) - \phi_2 - E'^\circ) \tag{15}$$

The double-layer potential also depends on the electrode potential, and decreased particle diameter will shift ϕ_2 to more negative values due to increasingly negative electron redox potentials. Inclusion of ϕ_2 and its size dependence in (8) and the Tafel plot of Figure 6 would shift the apparent α closer to 0.5. Also, the ionic strength and potential independent rate constant, k_t°, would be less than k'°. In related work, Matsumoto *et al.*[19] measured $\alpha' < 0.5$ for electron transfer from polyphosphate-capped size-quantized CdS nanocrystals to methylviologen. In this system, double-layer corrections also would bring α' closer to 0.5. In contrast, for electron transfer from 100 Å TiO_2 to methyl viologen, where there is no specific adsorption of the reactant, α was found to be 0.52.[75] Therefore, the value of α' determined from Figure 6 probably reflects the importance of specific adsorption and double-layer effects in this system.

Plotted in Figure 7 are nitrate reduction rates as a function of NaCl concentration. Note that double-layer effects are reduced at higher ionic strength, yet the addition of NaCl decreases nitrate photoreduction monotonically for both negatively charged (carboxy-capped) and positively charged (amine-capped) particles. In the case of the negatively charged particles, ϕ_2 is more negative, which reduces the thermodynamic driving force for electron transfer[38,39] and decreases nitrate concentrations close to the particle surface. Therefore, it might be expected that higher ionic strength would reduce double-layer effects resulting in increased reduction rates. However, possibly due to the displacement of nitrate from the surface by Cl^-, the reaction rates decrease with increasing NaCl concentration. It has been observed for photolysis of chloroform on TiO_2 as well that Cl^- adsorption may reduce photocatalytic efficiencies.[46]

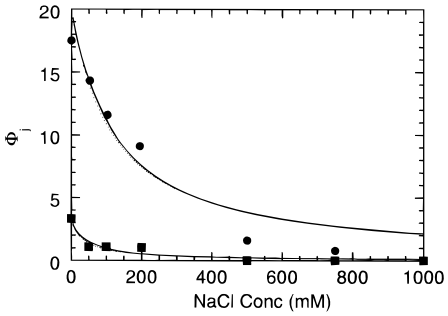

Figure 7. Current density quantum yield, Φ_j, versus sodium chloride concentration for positively (●, 21.2 Å, 75 mM nitrate, 75 mM formate) and negatively (■, 24.1 Å, 300 mM nitrate, 250 mM formate) charged CdS nanocrystals. The curve fits correspond to competitive adsorption fits assuming that formate competition is negligible.

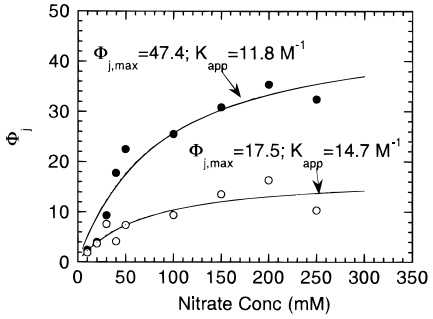

Figure 8. Current density quantum yield, Φ_j, versus nitrate concentration for amine-capped particles with diameters (●) 19.7 Å and (○) 21.7 Å. The curves represent the fit for the data using the Langmuir−Hinschelwood rate expression (20), which assumes that the reaction rate is limited by the adsorbed nitrate.

(ii) Adsorption Effects. As shown in Figure 8, Φ_j increases nonlinearly with increasing nitrate concentration, suggesting a role of adsorption in the observed kinetics. Many reactions photocatalyzed by semiconductor nanocrystals are controlled by adsorbed reactant concentrations.[1,3,4] In fact, it has been proposed that reactants must be preadsorbed prior to excitation in order to elicit efficient electron transfer rates, because electron−hole recombination is extremely fast in a semiconductor nanocrystal (tens to hundreds of picoseconds).[40] It is plausible that reactant adsorption affects nitrate photoreduction by quantum-sized CdS nanocrystals as well—especially when considering that negatively charged particles yield much reduced reactivity compared to positively charged particles. Relative success for describing, at least qualitatively,[49] the importance of substrate preadsorption on photocatalytic reaction rates has been achieved using a Langmuir−Hinschelwood rate analysis.[1,3,4,39,43,44] By assuming that the rate is proportional to the surface coverage, θ, the current density quantum yield, Φ_j, can be expressed as a function of the maximum current density quantum yield, $\Phi_{j,max}$, occurring for complete reactant coverage of the surface,

$$\Phi_j = \Phi_{j,max}\theta \tag{16}$$

Assuming Langmuir adsorption, θ is related to the bulk reactant concentration, C, by an apparent binding constant, K_{app},

$$\theta = K_{app}C/(1 + K_{app}C) \tag{17}$$

where K_{app} is a measure of the binding strength of a reactant for a particular surface. Therefore, a negatively charged reactant will have a smaller K_{app} for a negatively charged surface than for a positively charged surface. Substituting (17) into (16) gives the typical Langmuir−Hinschelwood (L−H) rate expres-

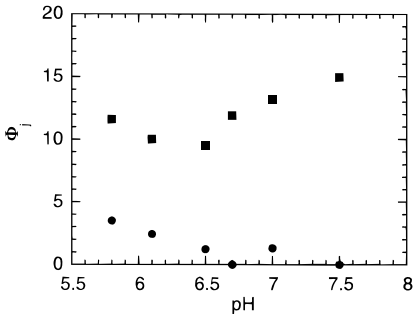

Figure 9. Current density quantum yield, Φ_j, versus solution pH for positively (■, 21.2 Å) and negatively (●, 24.2 Å) charged surfaces with 100 mM nitrate and 250 mM formate.

sion for a photocatalytic system,

$$\Phi_j = \Phi_{j,\max} CK_{app}/(1 + CK_{app}) \qquad (18)$$

Equation 18 may be viewed as the combination of two limiting cases. At high surface coverage Φ_j is independent of the solution concentration, $\theta \cong 1$ and $\Phi_j = \Phi_{j,\max}$, and at low surface coverage Φ_j increases linearly with nitrate concentration, $\Phi_j = \Phi_{j,\max} K_{app} C$. Shown in Figure 8 is the fit for (18) to rates for amine-capped nanocrystals of two different sizes. Higher $\Phi_{j,\max}$ for the smaller particles results from increased thermodynamic driving force due to quantum confinement effects ($\Phi_{j,\max,19.7Å} = 47.4$, $\Phi_{j,\max,21.7Å} = 17.4$). K_{app} is approximately equal for the two samples as expected since they are capped with the same ligands: $K_{app,19.7Å} = 11.8\ M^{-1}$ (95% confidence limits: 9.6, 15.7 M^{-1}), $K_{app,21.7Å} = 14.7\ M^{-1}$ (95% confidence limits: 10.7, 21.0 M^{-1}).

The effect of added NaCl on nitrate reduction rates plotted in Figure 7 can also be analyzed using an L−H rate expression that includes competitive adsorption:

$$\Phi_j = \Phi_{j,\max} CK_{app}/(1 + CK_{app} + \sum_i C_i K_{app,i}) \qquad (19)$$

Fitting (19) to the data in Figure 7 based upon the L−H parameters found above for positively charged particles without including competitive formate binding, $\Phi_{j,\max} = 35$, $K_{app,NO_3} = 13.5\ M^{-1}$, and $K_{app,NaCl} = 20.0\ M^{-1}$. At higher NaCl concentrations the L−H model overestimates nitrate photoreduction for the amine-capped nanocrystals. This deviation may indicate that decreased ϕ_2 at higher ionic strength is decreasing E_{eff} in magnitude, indicating that both adsorption and charge double-layer effects at the particle surface influence nitrate photoreduction. The best fit for the carboxy-capped particles gave a binding constant for nitrate on the order of that for the amine-capped particles, with a much higher binding constant for NaCl: $\Phi_{j,\max} = 6.0$, $K_{app,NO_3} = 12.0\ M^{-1}$, and $K_{app,NaCl} = 60.0\ M^{-1}$. Therefore, any decreases in double-layer effects which could improve nitrate photoreduction are probably masked by increased NaCl on the carboxy-coated surfaces as well.

(iii) pH Effects. Figure 9 shows the strong effect of pH on the rate of nitrate reduction for both positively and negatively capped nanocrystals. The rather narrow pH range studied is substantially above the pK's for both nitric and nitrous acids, somewhat above the likely pK_a for the chemisorbed carboxylic acid, and well below the likely pK_a for the chemisorbed amine. Since the pK_a of the chemisorbed mercaptoethylamine likely is close to 10, the amine is positively charged over the pH range studied. Inductive effects of the thiolate substituent of the chemisorbed acid will reduce its pK_a somewhat from that characteristic for acetic acid (4.74); yet below pH 6, a substantial fraction of the acidic groups may be protonated, thereby reducing electrostatic repulsion of the nitrate which would result in improved current density quantum yield. Since the potential of the nitrate/nitrite couple as a function of pH equals $0.01 + 0.059(14 - \text{pH})$,[60] nitrate is reduced more readily at lower pH values, which also may explain partially the reproducible improvement in efficiency for both amine- and carboxy-terminated particles at lower pH.

Electrostatic repulsion between the carboxy-capped particles and nitrate apparently becomes sufficiently strong to eliminate nitrate reduction at pH 7.0 and above. However, rather unexpectedly, the efficiency of the amine-capped particles goes through a minimum at about pH 6.5 and displays a significant rate increase at higher pH. This result may be an indication of the importance of surface trapping effects on photocatalytic quantum yields.

Studies have indicated that increased solution pH significantly enhances the fluorescence quantum yield and results in enhanced electron transfer efficiency, possibly due to the elimination of surface traps at higher pH.[19,32] Since these traps decrease the electron redox potential and provide sites for enhanced electron−hole recombination, the elimination of surface traps by solution species could be extremely important. Others have obtained evidence that chemisorbed amines bind to lower energy sites or increase the electron density at the semiconductor surface, thereby improving fluorescence quantum yields as well.[30,31] Some combination of these effects could explain the results obtained with the amine-capped particles. The nearly unmeasurable photocatalytic activity of the carboxy-terminated nanocrystals may indicate, however, that the decrease in surface trapping at higher pH is insufficient to outweigh electrostatic repulsion between the particle surface and nitrate.

Conclusions

Using quantum-sized CdS nanocrystals, electron redox potentials can be tuned to sufficiently negative potential to enable nitrate reduction at neutral pH. Although nitrate photoreduction depends strongly on the particle size, the surface character plays a critical role as well. Significantly higher nitrate reduction rates are achieved using amine-terminated nanocrystals as opposed to the carboxy-terminated species due to favorable electrostatic interaction of nitrate with the positively charged amine-capped particles. Therefore, although the role of the particle size is to set the thermodynamic driving force for electron transfer, the nanocrystal surfaces must be engineered such that they promote reactant adsorption in order to achieve efficient photoreduction. It remains a disappointment that despite the increase in band gap of these size-quantized CdS nanocrystals, the water oxidation rate is insufficient to compete with the photocorrosion of the semiconductor and a ready electron donor, *i.e.*, formate, had to be added to the solution. Nevertheless, this study furthers the argument that appropriate size and surface engineering of size-quantized semiconductor particles may lead to effective photocatalytic systems for nitrate reduction that operate without the need for an electron donor other than water.

Acknowledgment. B.A.K. is grateful for a U.S. Department of Education Pollution Prevention Fellowship (Award P200A40732). The authors thank M. V. Ramakrishna for empirical pseudopotential model data for the ΔE_c of size-quantized CdS nanoparticles.

References and Notes

(1) Fox, M. A.; Dulay, M. T. *Chem. Rev.* **1993**, *93*, 341−357.
(2) Henglein, A. *Top. Curr. Chem.* **1988**, *143*, 113−180.

(3) Kamat, P. V. *Chem. Rev.* **1993**, *93*, 267−300.
(4) Hoffman, M. R.; Martin, S. T.; Choi, W.; Bahnemann, D. W. *Chem. Rev.* **1995**, *95*, 69−96.
(5) Hagfeldt, A.; Grätzel, M. *Chem. Rev.* **1995**, *95*, 49−68.
(6) (a) Berry, C. R. *Phys. Rev.* **1967**, *161*, 848−851. (b) Brus, L. E. *J. Phys. Chem.* **1986**, *90*, 2555−2560. (c) Éfros, AI. L.; Éfros, A. L. *Fiz. Tekh. Poluprovodn.* **1982**, *16*, 1209 (*Sov. Phys. Semicond.* **1982**, *16*, 772).
(7) (a) Steigerwald, M. L.; Brus, L. E. *Annu. Rev. Mater. Sci.* **1988**, *19*, 471. (b) Stucky, G. D.; Mac Dougall, J. E. *Science* **1990**, *247*, 669. (c) Wang, Y.; Herron, N. *J. Phys. Chem.* **1991**, *95*, 525−532. (d) Weller, H. *Adv. Mater.* **1993**, *5*, 88. (e) Weller, H. *Angew. Chem., Int. Ed. Engl.* **1993**, *32*, 41. (f) Alivisatos, A. P. *Science* **1996**, *271*, 933−937.
(8) Brus, L. E. *J. Chem. Phys.* **1983**, *79*, 5566−5571.
(9) Hoyer, P.; Weller, H. *Chem. Phys. Lett.* **1994**, *221*, 379−384.
(10) Grätzel, M. In *Photocatalysis−Fundamentals and Applications*; Serpone, N., Pelizzetti, E., Eds.; Wiley-Interscience: New York, 1989; pp 123−157.
(11) Vogel, R.; Hoyer, P.; Weller, H. *J. Phys. Chem.* **1994**, *98*, 3183−3188.
(12) Fotjik, A.; Weller, H.; Koch, U.; Henglein, A. *Ber. Bunsen-Ges. Phys. Chem.* **1984**, *88*, 969−977.
(13) Hoffman, A. J.; Yee, H.; Mills, G.; Hoffmann, M. R. *J. Phys. Chem.* **1992**, *96*, 5540.
(14) Hoffman, A. J.; Hoffman, M. R. In *Photocatalytic Purification and Treatment of Water and Air*; Ollis, D. F., Al-Ekabi, H., Eds.; Elsevier Science Publishers B. V.: Amsterdam, 1993; pp 155−162.
(15) Nedelijkovic, J. M.; Nanadovic, M. T.; Micic, O. I., Nozik, A. J. *J. Phys. Chem.* **1986**, *90*, 12−13.
(16) Micic, O. I.; Rajh, T.; Nedeljkovic, J. M.; Comor, M. I. *Isr. J. Chem.* **1993**, *33*, 59.
(17) Motte, L.; Petit, C.; Boulanger, L.; Lixon, P.; Pileni, M. P. *Langmuir* **1992**, *8*, 1049−1053.
(18) Matsumoto, H.; Matsunaga, T.; Sakata, T.; Mori, H.; Yoneyama, H. *Langmuir* **1995**, *11*, 4283−4287.
(19) Matsumoto, H.; Uchida, H.; Matsunaga, T.; Tanaka, K.; Sakata, T.; Mori, H.; Yoneyama, H. *J. Phys. Chem.* **1994**, *98*, 11549−11556.
(20) Anpo, M.; Shima, T.; Kodama, S.; Kubokawa, Y. *J. Phys. Chem.* **1987**, *91*, 4305−4310.
(21) Shiragami, T.; Fukami, S.; Pac, C.; Yanagida, S. *J. Chem. Soc., Faraday Trans.* **1993**, *89*, 1857−1860.
(22) Yanagida, S.; Tomoyuki, O.; Shindo, A.; Hosokawa, H.; Mori, H.; Sakata, T.; Wada, Y. *Bull. Chem. Soc. Jpn.* **1995**, *68*, 752−758.
(23) Yanagida, S.; Yoshiya, M.; Shiragami, T.; Pac, C.; Mori, H.; Fujita, H. *J. Phys. Chem.* **1990**, *94*, 3104.
(24) Kanemoto, M.; Shiragami, T.; Pac, C.; Yanagida, S. *J. Phys. Chem.* **1992**, *96*, 3521.
(25) Chang, A.-C.; Fendler, J. H. *J. Phys. Chem.* **1989**, *93*, 2538.
(26) Wazke, H. J.; Fendler, J. H. *J. Phys. Chem.* **1987**, *91*, 854.
(27) Torimoto, T.; Uchida, H.; Sakata, T.; Mori, H.; Yoneyama, H. *J. Am. Chem. Soc.* **1993**, *115*, 1874−1880.
(28) Kamat, P. V.; Dimitrijevic, N. M.; Fessenden, R. W. *J. Phys. Chem.* **1987**, *91*, 396−401.
(29) Alivisatos, A. P.; Harris, A. L.; Levinos, N. J.; Steigerwald, M. L.; Brus, L. E. *J. Chem. Phys.* **1988**, *89*, 4001.
(30) Kamat, P. V.; de Lind van Wijngaarden, M.; Hotchandani, S. *Isr. J. Chem.* **1993**, *33*, 47−51.
(31) Dannhauser, T.; O'Neil, M.; Johansson, K.; Whitten, D.; McLendon, G. *J. Phys. Chem.* **1986**, *90*, 6074−6076.
(32) Spanhel, L.; Haase, M.; Weller, H.; Henglein, A. *J. Am. Chem. Soc.* **1987**, *109*, 5649−5655.
(33) Nosaka, Y.; Fox, M. A. *Langmuir* **1987**, *3*, 1147.
(34) Rajh, T.; Rabani, J. *Langmuir* **1991**, *7*, 2054−2059.
(35) Inoue, H.; Nakamura, R.; Yoneyama, H. *Chem. Lett.* **1994**, 1227−1230.
(36) Resch, U.; Eychmüller, A.; Haase, M.; Weller, H. *Langmuir* **1992**, *8*, 2215−2218.
(37) Colvin, V. L.; Goldstein, A. N.; Alivisatos, A. P. *J. Am. Chem. Soc.* **1992**, *114*, 5221.
(38) Uchihara, T.; Matsumura, M.; Ono, J.; Tsubomura, H. *J. Phys. Chem.* **1990**, *94*, 415−418.
(39) Kamat, P. V.; Dimitrijevic, N. M. *J. Phys. Chem.* **1989**, *93*, 4259−4263.
(40) Matthews, R. W. *J. Catal.* **1988**, *113*, 549.
(41) Rossetti, R.; Brus, L. E. *J. Phys. Chem.* **1986**, *90*, 558−560.
(42) Lewis, N. S. *Annu. Rev. Phys. Chem.* **1991**, *42*, 543−580.
(43) Inoue, H.; Ichiroku, N.; Torimoto, T.; Sakata, T.; Mori, H.; Yoneyama, H. *Langmuir* **1994**, *10*, 4517−4522.
(44) Moser, J.; Punchihewa, S.; Infelta, P. P.; Grätzel, M. *Langmuir* **1991**, *7*, 3012−3018.
(45) Brown, G. T.; Darwent, J. R.; Fletcher, P. D. I. *J. Am. Chem. Soc.* **1985**, *107*, 6446−6451.
(46) Kormann, C.; Bahnemann, D. W.; Hoffmann, M. R. *Environ. Sci. Technol.* **1991**, *25*, 494−500.
(47) Grabner, G.; Quint, R. M. *Langmuir* **1991**, *7*, 1091−1096.
(48) Duonghong, D.; Ramsden, J.; Grätzel, M. *J. Am. Chem. Soc.* **1982**, *104*, 2977−2985.
(49) Turchi, C. S.; Ollis, D. F. *J. Catal.* **1990**, *122*, 178−192.
(50) Barker, G. C. *Ber. Bunsen-Ges. Phys. Chem.* **1971**, *75*, 728.
(51) Benderskii, V. A.; Krivenko, A. G.; Ponomarev, E. A. *Dokl. Akad. Nauk SSSR* **1989**, *308*, 1159−1163.
(52) Taniguchi, I.; Nakashima, N.; Yasukouchi, K. *J. Chem. Soc., Chem. Commun.* **1986**, 1814−1815.
(53) Moyer, B. A.; Meyer, T. J. *J. Am. Chem. Soc.* **1979**, *101*, 1326−1328.
(54) Kuwambata, S.; Uezumi, S.; Tanaka, K.; Tanaka, T. *Inorg. Chem.* **1986**, *25*, 3018−3022.
(55) Huang, H.; Zhao, M.; Xing, X.; Bae, I. T.; Scherson, D. *J. Electroanal. Chem.* **1990**, *293*, 279−284.
(56) Xing, X.; Scherson, D. A. *J. Electrochem. Soc.* **1990**, *137*, 2166−2175.
(57) Willner, I.; Riklin, A.; Lapidot, N. *J. Am. Chem. Soc.* **1990**, *112*, 6438−6439.
(58) Mellor, R. B.; Ronnenberg, J.; Campbell, W. H.; Diekmann, S. *Nature* **1992**, *355*, 717−719.
(59) Suslick, K. S.; Watson, R. A. *Inorg. Chem.* **1991**, *30*, 912−919.
(60) Frank, A. J.; Grätzel, M. *Inorg. Chem.* **1982**, *21*, 3834−3837.
(61) Ohtani, B.; Kakimoto, M.; Miyadzu, H.; Nishimoto, S.; Kagiya, T. *J. Phys. Chem.* **1988**, *92*, 5773−5777.
(62) Halmann, M.; Tobin, J.; Zuckerman, K. *J. Electroanal. Chem.* **1986**, *209*, 405−411.
(63) Kudo, A.; Domen, K.; Maruya, K.; Onishi, T. *Chem. Lett.* **1987**, 1019−1022.
(64) Ranjit, K. T.; Krishnamoorthy, R.; Viswanathan, B. *J. Photochem. Photobiol. A: Chem.* **1994**, *81*, 55−58.
(65) Kudo, A.; Domen, K.; Maruya, K.; Onishi, T. *J. Catal.* **1992**, *135*, 300−303.
(66) Willner, I.; Lapidot, N.; Riklin, A. *J. Am. Chem. Soc.* **1989**, *111*, 1883−1884.
(67) Nosaka, Y.; Ohta, N.; Fukuyama, T.; Fujii, N. *J. Colloid Interface Sci.* **1993**, *155*, 23−29.
(68) Wegner, E. E.; Adamson, A. W. *J. Am. Chem. Soc.* **1966**, *88*, 394.
(69) Nicholas, D. D. J.; Nason, A. *Methods Enzymol.* **1957**, *3*, 983−984.
(70) Ramakrishna, M. V.; Friesner, R. A. *J. Chem. Phys.* **1991**, *95*, 8309.
(71) Korgel, B. A.; Monbouquette, H. G. *J. Phys. Chem.* **1996**, *100*, 346−351.
(72) Vossmeyer, T.; Katsikas, L.; Giersig, M.; Popovic, I. G.; Diesner, K.; Chemsiddine, A.; Eychmüller, A.; Weller, H. *J. Phys. Chem.* **1994**, *98*, 7665−7673.
(73) Tomasulo, A.; Ramakrishna, M. V. Unpublished results.
(74) Lippens, P. E.; Lannoo, M. *Phys. Rev. B* **1989**, *39*, 10935−10942.
(75) Grätzel, M.; Frank, A. J. *J. Phys. Chem.* **1982**, *86*, 2964−2967.
(76) Bard, A. J.; Faulkner, L. R. *Electrochemical Methods: Fundamentals and Applications*; John Wiley & Sons: New York, 1980.
(77) Wang, Y.; Harmer, M.; Herron, N. *Isr. J. Chem.* **1993**, *33*, 31−39.
(78) Forbes, M. D. E.; Lewis, N. S. *J. Am. Chem. Soc.* **1990**, *112*, 3682−3683.
(79) Pollock, D. D. *Physics of Engineering Materials*; Prentice Hall: Englewood Cliffs, NJ, 1990; p 485. In this case the electron density, N_c, is equal to the density of photon-generated electrons, n_{pge}, which for the steady-state case is equal to $1/V$, where V is the nanocrystal volume.
(80) Since a value for k_n ($=4 \times 10^{-3}$ cm/s) was reported in ref 75, k° was calculated using (9) and (10) with the reported value of $[MV^{2+}] = 6 \times 10^{17}$ molecules/cm^3 and $n_{so} = 3600$ cm^{-3} as calculated in ref 10. τ was calculated using (12) assuming that the characteristic dimension, d, for electron transfer is 10 Å as discussed in ref 42.
(81) Nosaka, Y.; Fox, M. A. *J. Phys. Chem.* **1986**, *90*, 6521−6522.
(82) Stryer, L. *Biochemistry*; W. H. Freeman: New York, 1988; p 191.
(83) Bennett, B.; Bray, R. C. *Biochem. Soc. Trans.* **1993**, *22*, 78S.